International Journal of Smart Home
Vol. 10, No.1, (2016), pp. 217-242
http://dx.doi.org/10.14257/ijsh.2016.10.1.21

A Novel Time of Arrival Estimation Algorithm based on Energy Detector

Xiao-Lin Liang[1], Hao Zhang[1, 2], Ting-Ting Lu[1], Luji Cui[1], T. Aaron. Gulliver[2] and Meng Zhang[1]

[1]*College of Information Science and Engineering, Ocean University of China, Qingdao, 266100, China*
[2]*Department of Electrical and Computer Engineering, University of Victoria, Victoria V8W 3P6, Canada*
xiaolin87liang@163.com,zhanghao@ouc.edu.cn, lvtingting33@163.com, cuiluji@126.com agullive@ece.uvic.ca, zhangmeng7526@126.com

Abstract

Accurate localization has gained significant interest in the field of sensor networks, impulse radio60GHz signals which is low cost, low complexity are even much more practical for ranging, localization and tracking systems because of the high time and multipath resolution and so on. Typically, accurate Time of Arrival (TOA) estimation of the 60GHz signals is very important. In order to improve the precision of the TOA estimation, a new TOA estimation algorithm based on Energy Detector is proposed which is based on a joint metric of the Skewness, Kurtosis, Maximum Slope and Standard Deviation after Energy Detection. The best threshold based on the signal-to-noise ratio (SNR) is investigated and the effects of the integration period and channel model are examined. Simulation results are presented which show that for theIEEE802.15.3c channel models CM1.1 and CM2.1, the proposed algorithm provides better precision and robustness in both high and low SNR environments than other ED-based algorithms.

Keywords: *60GHz, TOA estimation, Energy Detector, Skewness, Kurtosis, Maximum Slope and Standard Deviation*

1. Introduction

The demand for high data rate wireless communications with low latency has increased dramatically in recent years. Unfortunately, due to spectrum limitations and transmit power regulations, current short-range wireless communication strategies cannot achieve Gigabit per second (Gbps) data rates. Fortunately, wireless communications in the 60GHz millimeter wave (mm-wave) band has become viable for Gbps wireless communication networks [1-4] due to the availability of several GHz of license-free spectrum, up to 10W maximum transmit power, no interference from other systems, and the development of low-cost Complementary Metal-Oxide Semiconductor (CMOS) devices.

The Federal Communications Commission (FCC) permits communications in the 60GHz unlicensed band at an Effective Isotropic Radiated Power (EIRP) of up to 40dBm, which is many times greater than other short-range wireless communication strategies. In China, this limit is 44dBm [5]. Although the Path Loss (PL) is high at 60GHz, the received power can still be significant. Impulse radio (IR) communication strategies have been proposed for this frequency band because it can be effective in separating the multipath signals at the receiver. This is because short pulses are employed for communications with a duration (typically under 100 picoseconds), which is far less than the multipath propagation delay. These signals can also provide the fine multipath

ISSN: 1975-4094 IJSH

resolution required for high precision ranging and localization [6].Thus, 60GHz signals are even much suitable for localization applications for short distances.

Generally, the localization strategies can be classified into range based[7-10] and non-range based [11]. For example, TOA [10, 12] and Time Difference of Arrival (TDOA) [10] are range based strategies, while Received Signal Strength (RSS) and Angle of Arrival(AOA) [11] are non-range based. Localization that based on range (TOA or TDOA) is even much suitable for usingwithIR-60GHzstrategy [11], as it can take full advantage of the higher time and multipath resolution available with very short IR-60GHzsignals. TOA estimation which is even much more accurate is the key to accurate ranging, but this is very challenging due to the potentially hundreds of multipath components in 60GHz channels, even in the Non-line of Sight (NLOS) environments.

TOA estimation has been extensively studied [12, 15-18] for the past few years. There are two approaches which are much more applicable for TOA estimation, a Matched Filter [16] (such as a rake or correlation receiver) with a higher sampling rate and higher precision correlation, or an Energy Detector [18] with a lower sampling rate and lower complex. A Matched Filter is the optimal strategy for TOA estimation, where a correlator template is matched exactly to the received signal. However, a receiver operating at the NY Quist sampling rate makes it very difficult to align with the multipath components of the received signal [15].

In addition, a Matched Filter requires a priori estimation of the channel, including the timing, fading coefficient, and pulse shape for each component of the impulse response [15]. Because of the higher sampling rates and channel estimation, a Matched Filter may not be practical in many applications. As opposed to a more complex Matched Filter, an Energy Detector is a non-coherent approach to TOA estimation. It consists of a square-law device, followed by an integrator, sampler and a decision mechanism. The TOA estimate is made by comparing the integrator output with a threshold and choosing the first sample to exceed the threshold. This is a convenient strategy that directly yields an estimate of the start of the received signal. Thus, a low complexity, low sampling rate receiver can be employed without the need for a priori channel estimation.

The major challenge with Energy Detector is the selection of an appropriate threshold based on the received signal samples. In [17], a normalized threshold selection strategy for TOA estimation was proposed which exploits the kurtosis of the received samples. In [18], an approach based on the minimum and maximum sample energy was introduced. Threshold selection for different SNR values was investigated via simulation. These approaches have limited TOA precision, as the strongest path is not necessarily the first arriving path.

In this paper, we consider the relationship between the SNR and the statistics of the integrator output including Maximum Slope, Kurtosis, Skewness and Standard Deviation. A metric based on Maximum Slope, Kurtosis, Skewness and Standard Deviation is then developed for threshold selection. The threshold for different SNR values is investigated and the effects of the integration period and channel are examined. Performance results are presented which show that in both the CM1.1 and CM2.1 channels, this joint metric provides higher precision and robustness.

The remainder of this paper is organized as follows. In Section 2 the system model is outlined. Section 3discusses various TOA estimation algorithms based on Energy Detector. Section 4 considers the statistical characteristics of the energy values. In Section 5 a joint metric based on Maximum Slope, Kurtosis, Skewness and Standard Deviation is proposed. Some performance results are presented in Section 6 and Section 7 concludes the paper.

2. System Model

Currently, there are two important standards that have been developed for 60GHz wireless communications systems, IEEE 802.15.3c and IEEE 802.11ad [19-20]. In this paper, the channel models in IEEE 802.15. 3c standard are used because it is specifically designed for Wireless Personal Area Networks and thus encompasses typical indoor environments. Further, these are the most widely employed models for 60GHz systems. The IEEE 802.15.3c standard was the first developed for high data rate short-range wireless systems. The physical layer was designed to support the transmission of data within a few meters at a minimum data rate of 2Gbps. These models have been developed for communications in the frequency band 57 to 66GHz in indoor residential, indoor office and library environments (with differences largely due to the LOS and NLOS characteristics) [21-25].

In this paper, a Pulse Position Modulation Time Hopping60GHz signal is employed for ranging purposes. The propagation delay $\hat{\tau}$, between the transmitter and receiver is estimated for use in localization.

2.1. 60GHz Signal

The 2PPM-TH-60GHz signals have a very short duration (typically 100 picoseconds or less), and can be expressed as

$$s(t) = \sum_{-\infty}^{\infty} p\left(t - jT_s - C_j T_c - a_j \varepsilon\right) \quad (1)$$

Each symbol is represented by a sequence of very short pulses, where T_s is the symbol time. The Time Hopping (TH) code represented by C is a pseudorandom integer-valued sequence which is unique for each user to limit multiple access interference, and T_c is the chip time. The PPM time shift is ε so that if a_j is 1, the signal is shifted in time by ε, while a_j is 0, there is no shift. In general, these parameters satisfy the following relationship:

$$(1)\, C_j T_c + \varepsilon < T_s ;\ (2)\, \varepsilon < T_c ;\ (3)\, a_j \varepsilon < C_j T_c \left(C_j \neq 0\right)$$

Many pulse shapes have been proposed for 60 GHz systems. In this paper a Gaussian pulse is employed which is multiplied by the carrier signal to give as shown in the Figure1 [26]

$$p(t) = \frac{\sqrt{2}}{\alpha} \exp\left(-2\pi \frac{t^2}{\alpha^2}\right) \cos\left(2\pi f_c t\right) \quad (2)$$

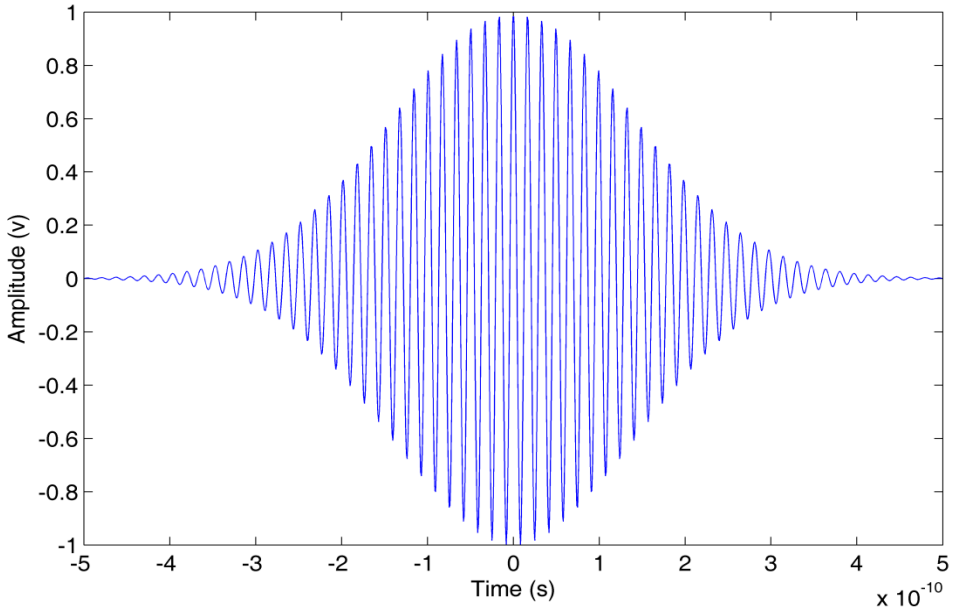

Figure 1. Waveform of the 60GHz Signal

Here α is the shape factor, and f_c is the carrier frequency which here is $f_c = 60$ GHz. A smaller shape factor results in a shorter duration pulse and a larger bandwidth.

2.2. Signal Shift and Path Loss

The path loss is defined as the ratio of the received signal power to the transmit signal power and it is very important for link budget analysis. Unlike narrow-band system, the path loss for a wide-band system such as mm-wave system is both distance and frequency dependent. In order to simplify the models, it is assumed that the frequency dependence path loss is negligible and only distance dependence path loss is modeled. The signal path loss, which depends on the propagation distance and the channel (IEEE802.15.3c), is described by

$$PL(d)[dB] = PL_0 + 10 \cdot n \log_{10}\left(\frac{d}{d_0}\right) + X_\sigma [dB];\ d \geq d_0 \quad (3)$$

Where d_0 and d denote the reference distance, and distance respectively. Thepath loss exponent n for mm-wave based measurements ranges from 1.2-2.0 for LOS and from 1.97-10 for NLOS, in various different indoor environments. In the presence of wave guiding effects and reverberation effects which lead to increase in power levels by multipath aggregation, n can be smaller than 2. X_σ is that the unit dB, with mean zero and variance σ_s for a Gaussian random variable [11]. Table 1 summarizes the values of n, PL_0, σ_s for different environments and scenarios.

Table1. Values of n, PL_0, σ_s for Different Environments and Scenarios

environments	*n*	PL_0	σ_s
Indoorresidential(LOS)	1.53	75.1	1.50
indoor residential(NLOS)	2.44	86.0	6.20
indoor office (LOS)	1.16	84.6	5.40
indoor office (NLOS)	3.74	56.1	8.60

The signal shift can be expressed as:

$$t = dt * floor\left((d / c)/dt\right) \tag{4}$$

Whered denotes the distance between the transmitter and receiver, dt is the sampling period and c is the speed of light which is 299792458m/s in the air.

2.3. Multipath Fading Channel

The received signal can be written as

$$r(t) = \sum_{n=1}^{N} \alpha_n p(t - \tau_n) + n(t) \tag{5}$$

Where N is the number of received multipath components, α_n and τ_n denotes the amplitude and delay of the nth path respectively, p (t) is the received 60GHz pulse and n (t)is Additive White Gaussian Noise (AWGN) with zero mean and two sided power spectral density N0/2. Equation (5)can be rewritten as

$$r(t) = s(t) * h(t) + n(t) \tag{6}$$

Where $s(t)$ is the transmitted signal, and $h(t)$ is the channel impulse response which can be expressed as

$$h(t,\theta) = \sum_{k=1}^{K} \sum_{l=1}^{L_k} \mu_{kl} \delta(t - T_k - \tau_{kl}) \delta(\theta - \theta_k - \omega_{kl}) \tag{7}$$

Where $\delta(.)$ is the Dirac-delta function, K is the number of clusters, L_k is the number of rays in the k^{th} cluster, and μ_{kl}, τ_{kl} and ω_{kl} denote the complex amplitude, delay and azimuth of the k^{th} ray of the l^{th} cluster, respectively. Similarly, T_k and θ_k represent the delay and mean Angle of Arrivalof the k^{th} cluster.

2.4. Energy Detector

As shown in Figure 2[27], after the amplifier, the received signals are squared, and then input to an integrator with integration period Tb. Because of the inter-frame leakage due to multipath signals, the integration duration is $3T_f / 2$, so the number of signal values for Energy Detector is N= $3T_f / 2Tb$. The integrator outputs can be expressed as:

$$z[n] = \sum_{i=1}^{N} \int_{(i-1)T_f + (c_j + n - 1)Tb}^{(i-1)T_f + (c_j + n)Tb} r^2(t) dt \tag{8}$$

Where $n \in \{1, 2, .., N\}$ denotes the sample index with respect to the starting point of the integration period and N is the number of pulses per symbol. Here, N is set to 1, so the integrator outputs are

$$z[n] = \sum_{i=1}^{N} \int_{(c_j + n - 1)Tb}^{(c_j + n)Tb} r^2(t) dt \tag{9}$$

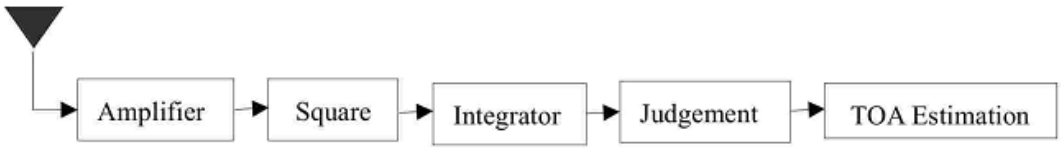

Figure 2. Block Diagram of the Energy Detector Receiver

If $z[n]$ is the integration of noise only, it has a centralized Chi-square distribution, while it has a non-centralized Chi-square distribution if a signal is present. The mean and variance of the noise and signal values are given by [17] respectively.

$$\mu_0 = F\sigma^2, \sigma_0 = 2F\sigma^4 \tag{10}$$

$$\mu_e = F\sigma^2 + E_n, \sigma_e^2 = 2F\sigma^4 + 4\sigma^2 E_n \quad (11)$$

Here E_n is the signal energy within the nth integration period and F is the number of degrees of freedom given by $F = 2BTb + 1$. Here B is the signal bandwidth.

3. TOA Estimation Based on Energy Detector

3.1. TOA Estimation Algorithms

There are many TOA estimation algorithms based on Energy Detector for determining the start block of a received signal. The simplest is Maximum Energy Selection (MES), which chooses the maximum energy value to be the start of the signal value. The TOA is estimated as the center of the corresponding integration period

$$\tau_{MES} = \left\lceil \left(\arg\max_{1 \le n \le N_b} \{ z[n] \} - 0.5 \right) \right\rceil Tb \quad (12)$$

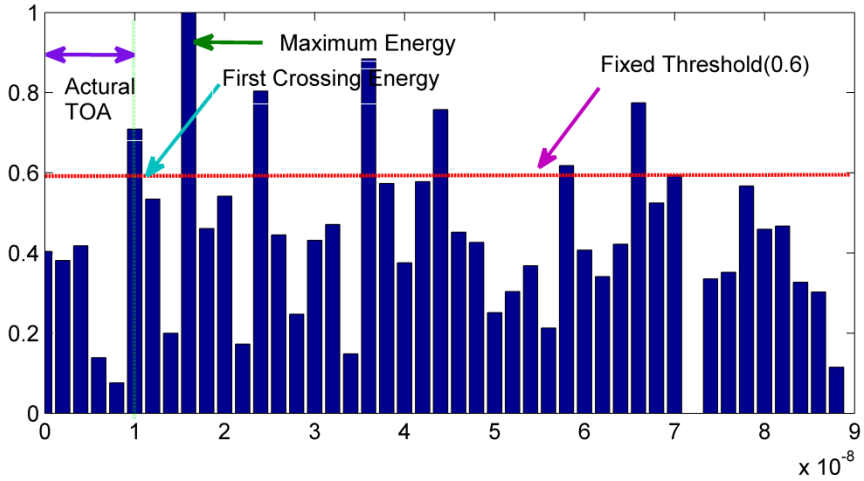

Figure 3. TOA Estimation Based on Energy Detector

However, as show in Figure 3, the maximum energy value may not be the first energy block [13], especially in NLOS environments. On average, the first energy value $z[n]$ is located before the maximum $z[n_{\max}]$, *i.e.*, $n \le n_{\max}$. Thus, Threshold Crossing TOA estimation has been proposed where the received energy values are compared to an appropriate threshold α. In this case, the TOA estimation is given by

$$\tau_{TC} = \left\lceil \left(\arg\min_{1 \le n \le n_{\max}} \{ n \mid z[n] \ge \xi \} - 0.5 \right) \right\rceil Tb \quad (13)$$

It is difficult to determine an appropriate threshold α directly, so usually a normalized threshold α_{norm} is calculated. Using α_{norm}, α is given by

$$\alpha = \alpha_{norm} \left(\max(z(n)) - \min(z(n)) \right) + \min(z(n)) \quad (14)$$

The TOA (τ_{TC}) is then obtained using (11).A simpler Threshold Crossing algorithm is the Fixed Threshold algorithm where the threshold is set to a fixed value, for example $\alpha_{norm} = 0.4$ .The problem in this case becomes one of how to set the threshold. It should be based on the statistics of the signal energy, particularly for multipath, NLOS indoor environments.

3.2. Error Analysis

The Mean Absolute Error (MAE) of TOA estimation based on Threshold Crossing was

analyzed, and closed form error expressions derived. The MAE can be used to evaluate the quality of an algorithm, and is defined as

$$MAE = \frac{1}{N}\sum_{n=1}^{N}\left(t_n - t_n\right) \tag{15}$$

Where t_n is the nth actual propagation time, t_n is the nth TOA estimate, and N is the number of TOA estimates.

4. Statistical Characteristics

Maximum Slope, Kurtosis, Skewness and Standard Deviation of the energy blocks are analyzed in this section.

4.1. Kurtosis

The Kurtosis is calculated using the second and fourth order moments and is given by

$$k = \frac{E\left[\left(x_i - \mu_x\right)^4\right]}{E\left[\left(x_i - \mu_x\right)^2\right]^2} = \frac{E\left[\left(x_i - \mu_x\right)^4\right]}{\sigma_x^4} \tag{16}$$

Here μ_x is the mean value, and σ_x is the standard deviation. The Kurtosis for a standard normal distribution is three. For this reason, Kurtosis is often redefined as $K = K - 3$ (often referred to as "excess Kurtosis"), so that the standard normal distribution has a Kurtosis of zero, positive Kurtosis indicates a "peaked" distribution and negative Kurtosis indicates a "flat" distribution. For noise only (or for a low SNR) and sufficiently large F (degrees of freedom of the Chi-square distribution), $z[n]$ has a Gaussian distribution and Kurtosis =0. On the other hand, as the SNR increases, Kurtosis will tend to increase.

4.2. Maximum Slope

Kurtosis cannot account for delay or propagation time, so the slope of the energy values is considered as a measure. These values are divided into (N-M+1) groups, with M values in each group. The slope for each group is calculated using a least squares line-fit. The Maximum Slope can then be expressed as

$$MS = \max_{1 \le n \le N-M+1} slope\left\{linefit\left(z[n], z[n+1], ..., z[n+M-1]\right)\right\} \tag{17}$$

4.3. Standard Deviation

The Standard Deviation is a widely used measure of variability. It shows how much variation or "dispersion" there is from the average (mean or expected value). The Standard Deviation is given by

$$D = \sqrt{\frac{\sum_{i=1}^{N}\left(x_i - \mu_x\right)^2}{N-1}} \tag{18}$$

4.4. Skewness

The Skewness is given by

$$S = \frac{1}{(N-1)\delta^3}\sum_{i=1}^{N}\left(x_i - \mu_x\right)^3 \tag{19}$$

Here μ_x is the mean value, and δ is the standard deviation of the energy values. The Skewness for a normal distribution is 0; in fact any symmetric data will have a Skewness of zero. Negative values of Skewness indicate that the data is skewed left, while positive values indicate data that is skewed right. Skewed left indicates that the left tail is long relative to the right tail, while skewed right indicates the opposite. For noise only (or very

low SNR), and sufficiently large F, Skewness≈0. As the SNR increases, Skewness will tend to increase.

4.5. Characteristics of Parameters

In order to examine the characteristics of parameters (Skewness, Maximum Slope, Kurtosis and Standard Deviation), the CM1.1 (residential LOS) and CM2.1 (residential NLOS) channel models from the IEEE802.15.3c standard are employed. For each SNR value, 1000 channel realizations are generated and sampled at $f_c = 1 \cdot e^{10}$ Hz. The other system parameters are $T_f = 200ns$, $T_c = 1ns$, the value of Tb is from1ns to 4nsand N=1. Each realization has a TOA uniformly distributed within $(0\ T_f)$.

The four parameters were calculated, and the results obtained are shown in from Figures 4-11. This results show that the characteristics of the parameters with respect to the SNR are similar for the two channels. Further, from Figures 4-11, results show that the Maximum Slope isn't monotonous with respect to SNR (especially in the NLOS environment) in the 60GHz wireless communication system. So the results of the multiplication of the two variables (Maximum Slope and Standard Deviation) are used as the new parameter 'SM'. By the same token, the results of the division of two variables (Kurtosis and Skewness) are used as the new parameter 'K/S'.

We can see that K/S, Skewness, Kurtosis increases as the SNR increases both in channel CM1.1 and CM2.1, but K/S changes more rapidly in comparison with other parameters. Conversely, the SM and Standard Deviation decrease with the increase of the SNR, but the SM changes more rapidly in comparison with other parameters. Since SM and K/S change more rapidly than other parameters, they better reflect changes in SNR, and so they are even more suitable for TOA estimation. Moreover, when the SNR is less than 10dB, K/S changes slowly while the SM changes rapidly. On the other hand, when the SNR is higher than 10dB, the SM changes rapidly but the K/S changes slowly. Therefore, no single parameter is a good measure of SNR change over a wide range of values. Thus, a joint metric based on Skewness,

Maximum Slope, Kurtosis and Standard Deviation are proposed in the next section for TOA estimation.

Based on the results in Section 4.5, a joint metric for TOA estimation is formulated as

$$G = K / S - SM \tag{20}$$

Where 'K/S' is the results of the division of two variables (Kurtosis and Skewness) and 'SM' is the results of the multiplication of the two variables (Maximum Slope and Standard Deviation).

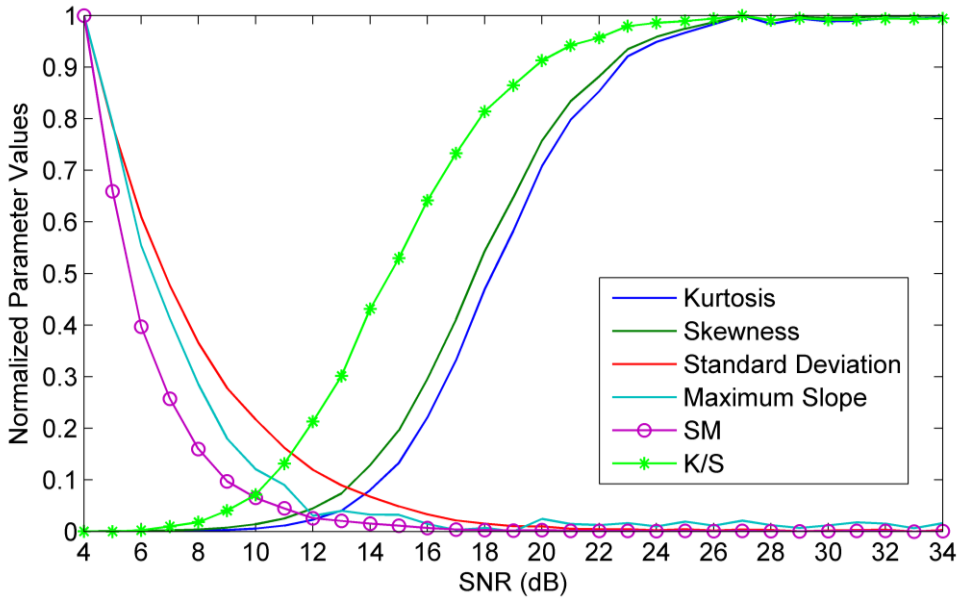

Figure 4. Parameters Change with SNR in CM1.1 with Tb=1ns

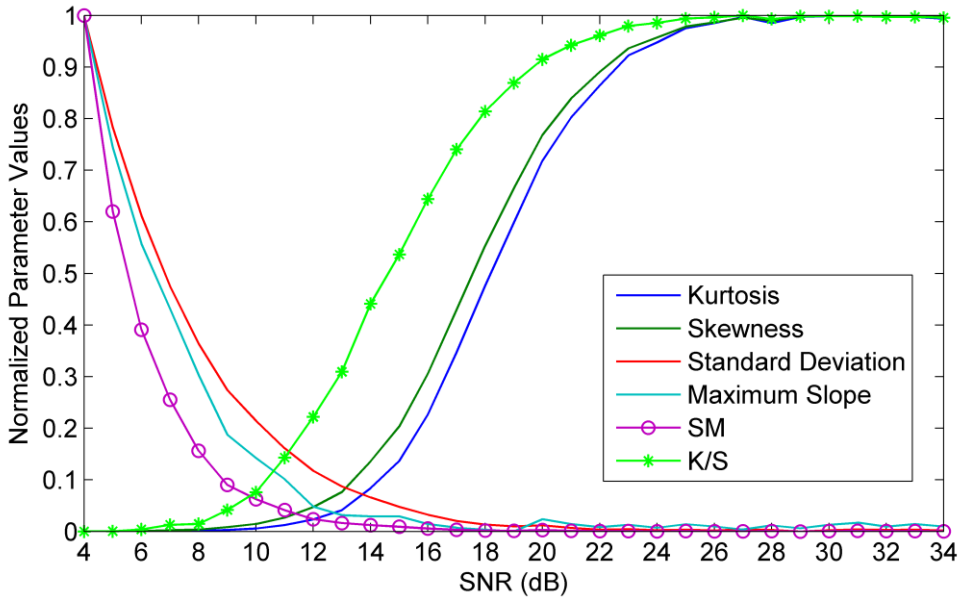

Figure 5. Parameters Change with SNR in CM1.1 with Tb=2ns

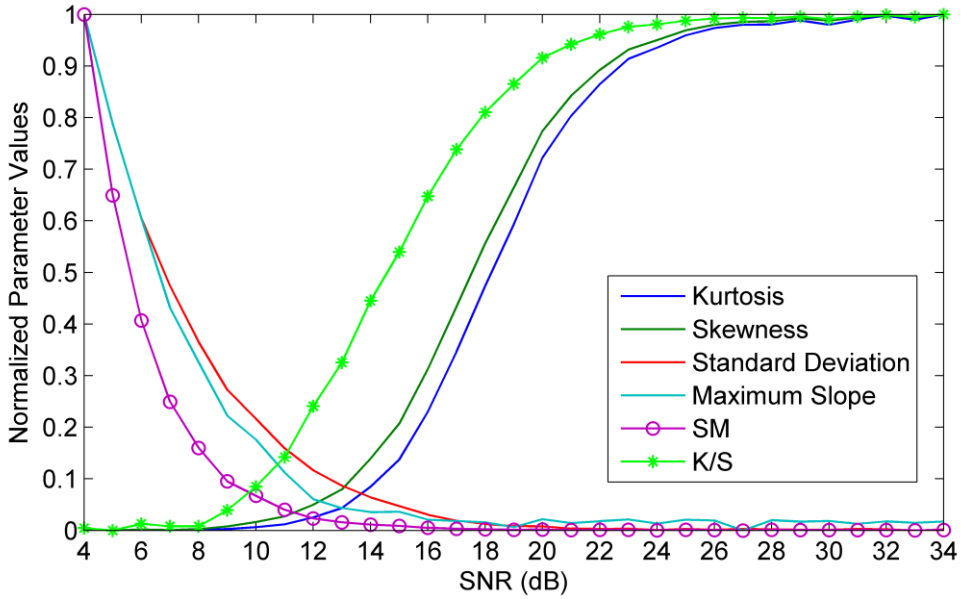

Figure 6. Parameters Change with SNR in CM1.1 with Tb=3ns

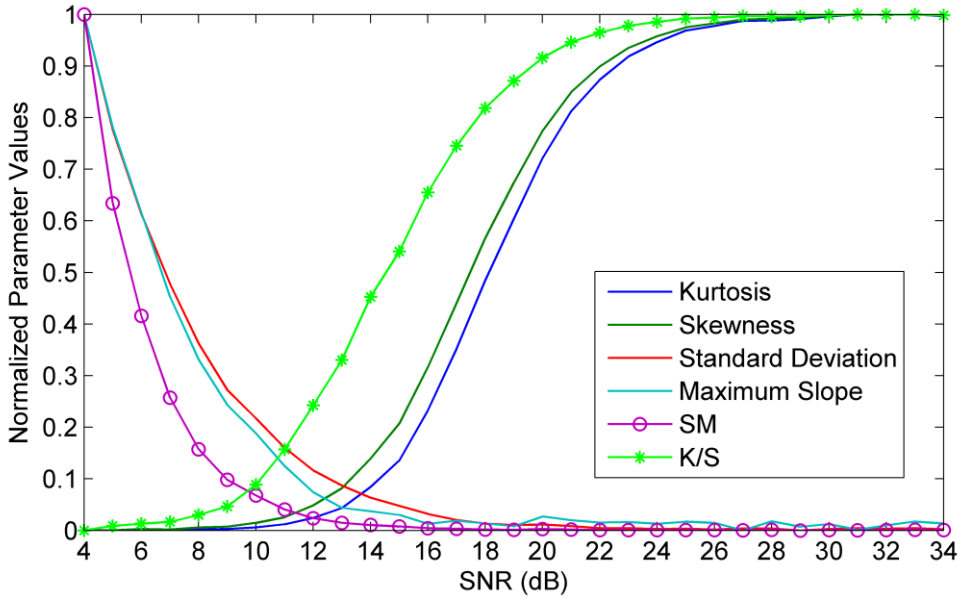

Figure 7. Parameters Change with SNR in CM1.1 with Tb=4ns

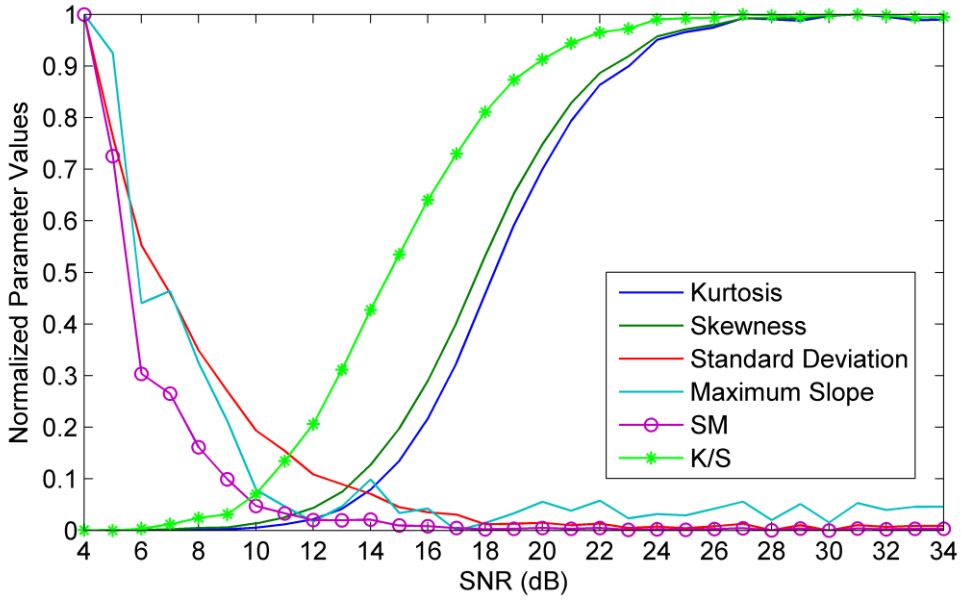

Figure 8. Parameters Change with SNR in CM 2.1 with Tb=1ns

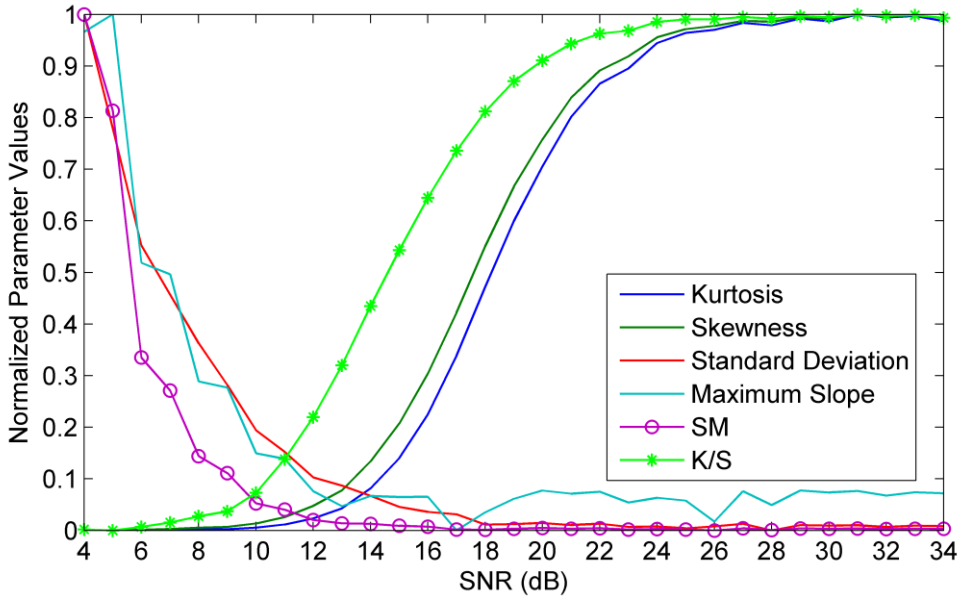

Figure 9. Parameters Change with SNR in CM 2.1 with Tb=2ns

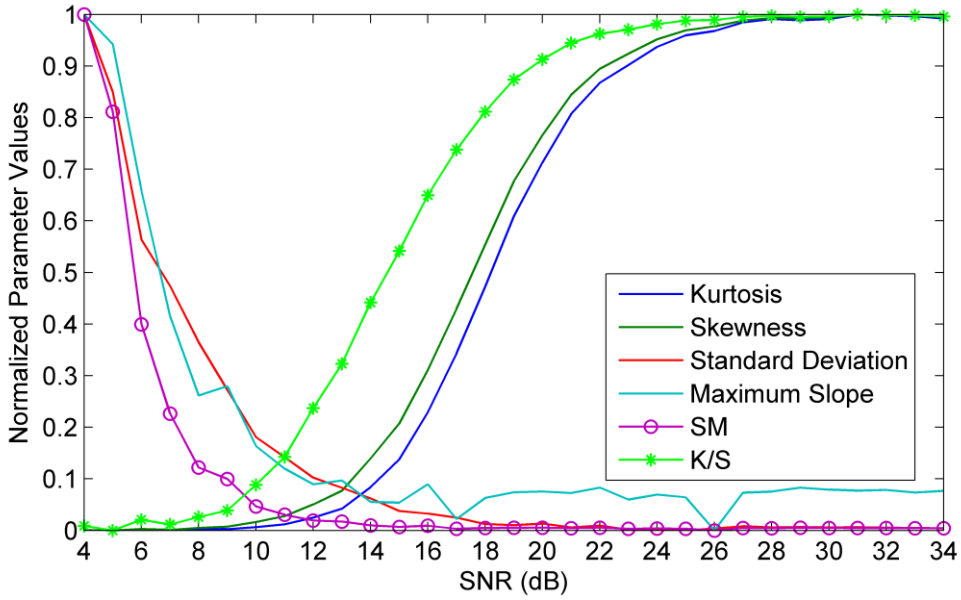

Figure 10. Parameters Change with SNR in CM 2.1 with Tb=3ns

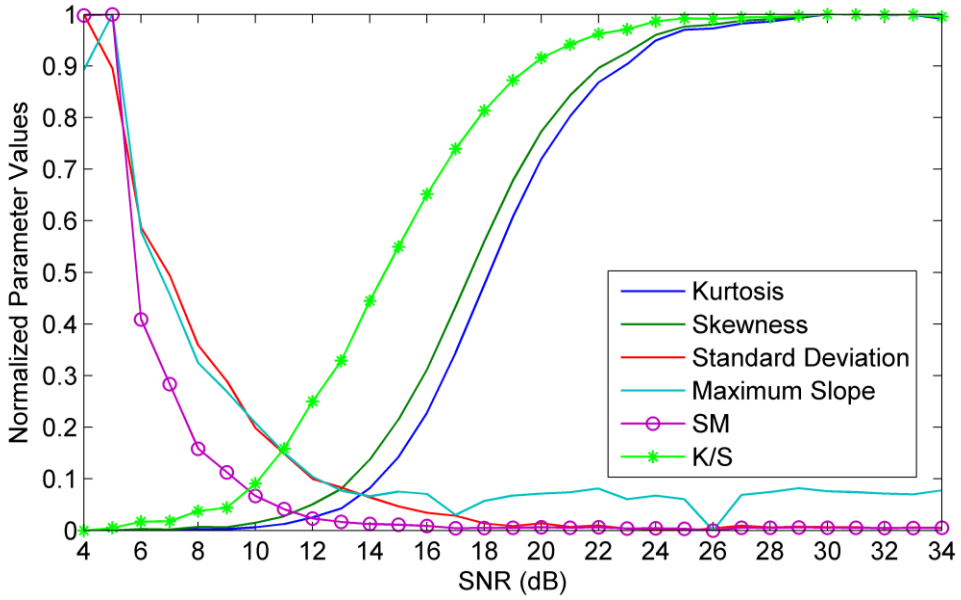

Figure 11. Parameters Change with SNR in CM 2.1 with Tb=4ns

5. Optimal Threshold Selection

The relationship between G and the optimal normalized threshold α_{opt} must be established. According to Figures 12 and 13, the curves forCM1.1 andCM2.1 for a given value of Tb are similar, so models are derived only for Tb=1ns, Tb=2ns, Tb=3ns and Tb=4ns. The steps to establish the relationship between G and α_{opt} can expressed as:

(1)Generating amounts of channel realizations (1000 channel realizations are generated in this paper) aiming at different channel model (CM1.1 and CM2.1), Tb=1ns, 2ns, 3ns and 4ns, and SNR value in the range from 4dB to 32dB.

(2) Calculating the average value of MAE with respect to different α_{norm} for different G value, channel model(CM1.1 and CM2.1), and Tb as shown inSection“5.2.Relationship

between MAE and the Normalized Threshold". In the process of simulation, because of the signals are generated randomly, so there are different MAE values with respect to one normalized threshold, so the average MAE is obtained. At the same time, because G is a real value, G should be rounded to the nearest discrete value, for example integer value or half-integer value.

(3) Selecting the normalized threshold with the lowest MAE as the best threshold α_{best} with respect to G for each channel model and Tb, as shown in Section "Optimal thresholds".

(4) Calculating the average normalized thresholds of channels CM1.1 and CM2.1 for different G as the optimal normalized threshold α_{norm}, as shown in Section "Optimal thresholds".

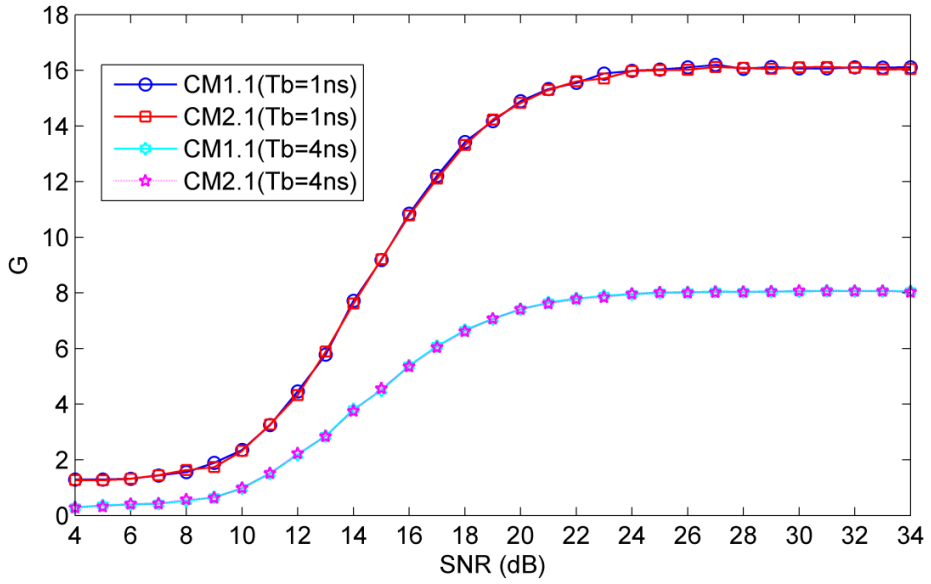

Figure 12. Average Values with Respect to SNR for Different CM and Tb

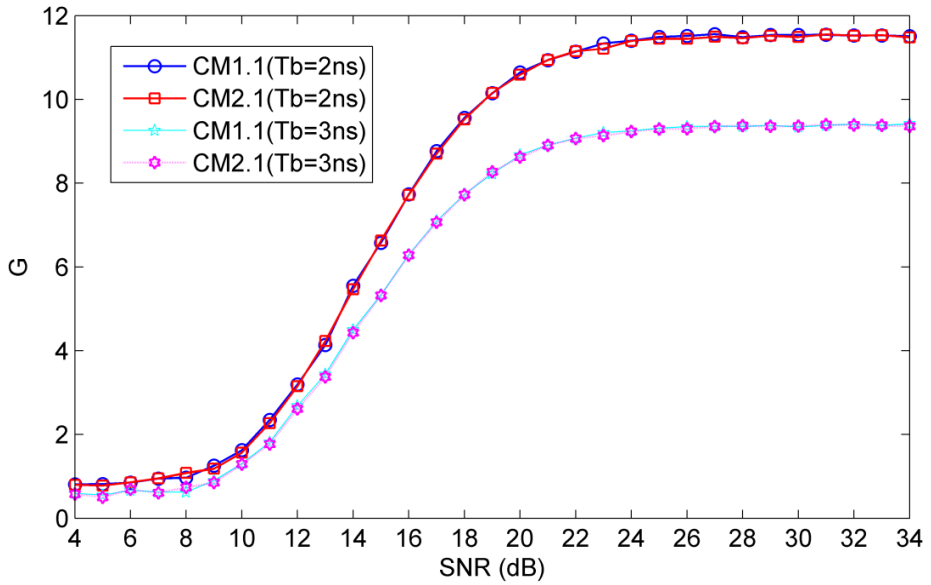

Figure 13. Average Values with Respect to SNR for Different CM and Tb

5.1. Relationship between G and SNR

In order to verify the relationship between the proposed metric G and SNR, 1000 channel realizations were generated when SNR is from 4 dB to 34 dB in eachIEEE802.15.3c channel. The average values of G are presented in the Figure 12 and Figure 13. The results show that G is a monotonic function for a large range of SNR values, and it is even much more sensitive to changes in SNR. The eight fixed curves differ somewhat due to the Channel Model and integration period used. The figure shows that G is more sensitive to T_b .

5.2. Relationship between MAE and the Normalized Threshold

In order to determine the best threshold (α_{best}) based on G, the relationship between MAE and normalized threshold (α_{norm}) was investigated. 1000 channel realizations with SNR={4, 5,⋯, 34} dB were simulated under CM1.1 and CM2.1 environments. α is the threshold which is compared to the energy values to find the first threshold crossing. When α is bigger than $z[n_{\max}]$, we can't get the TOA estimation, so in this case, α is set to be 1.

In the simulation, all G values were rounded to the nearest integer and half-integer values for all SNR values. From Figures14-21 show the relationship between MAE and the Normalized Threshold in the CM1.1 and CM2.1channels, respectively, with T_b is1ns, 2ns, 3ns and 4ns. The relationship is always that the MAE decreases as G increases. Another conclusion is that the minimum MAE is lower as G increases. The normalized threshold α_{norm} with respect to the minimum MAE is just the best threshold α_{best} . The relationship between α_{best} and G will be shown in the next section.

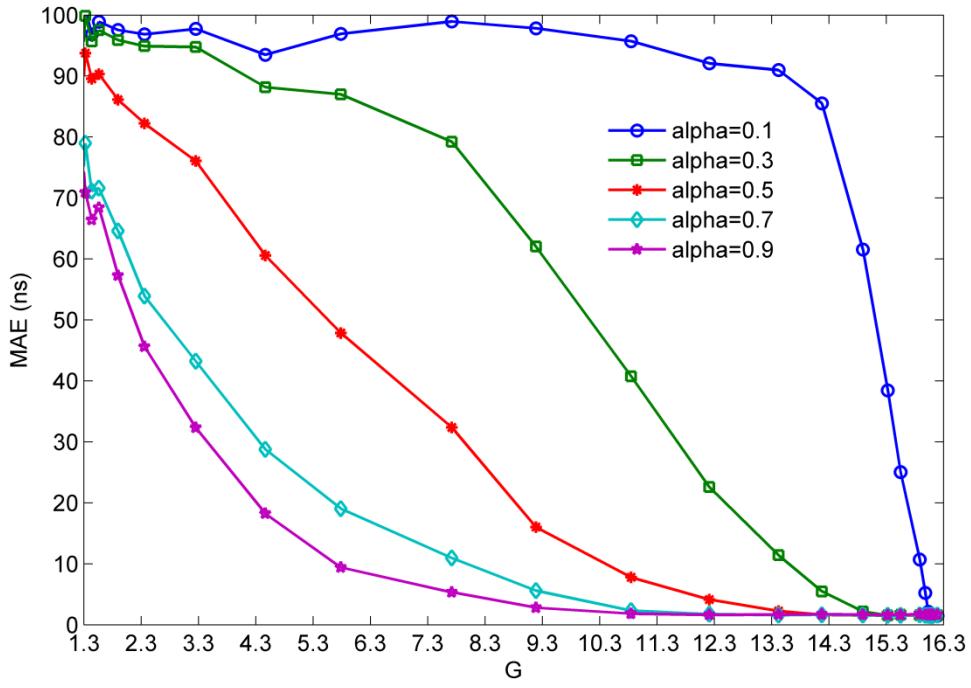

Figure 14. MAE with Respect to G (CM1.1 and Tb=1ns)

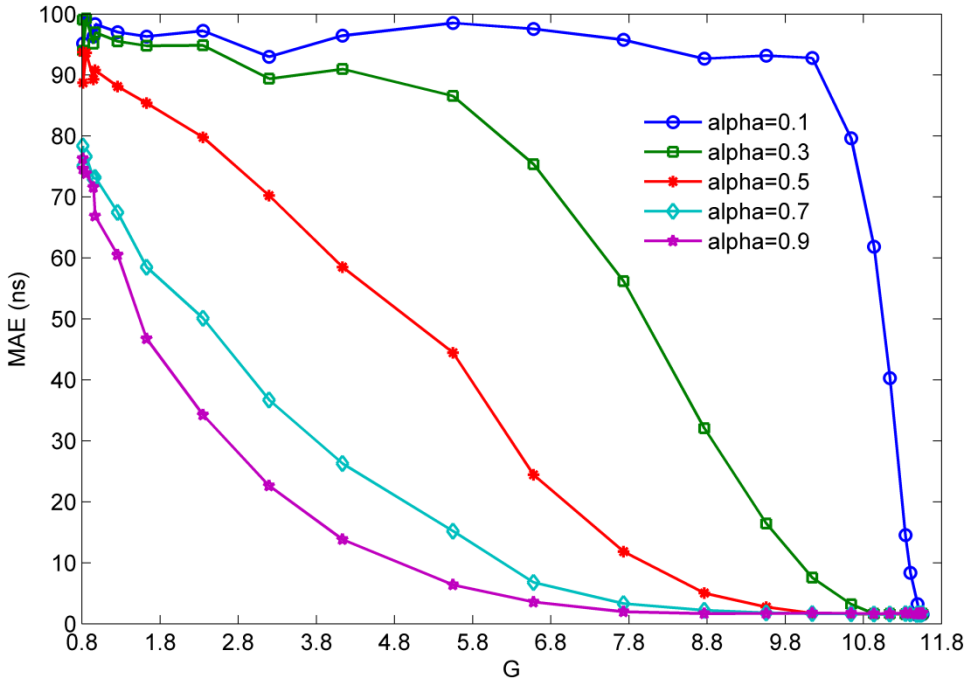

Figure 15. MAE with Respect to G(CM1.1 and Tb=2ns)

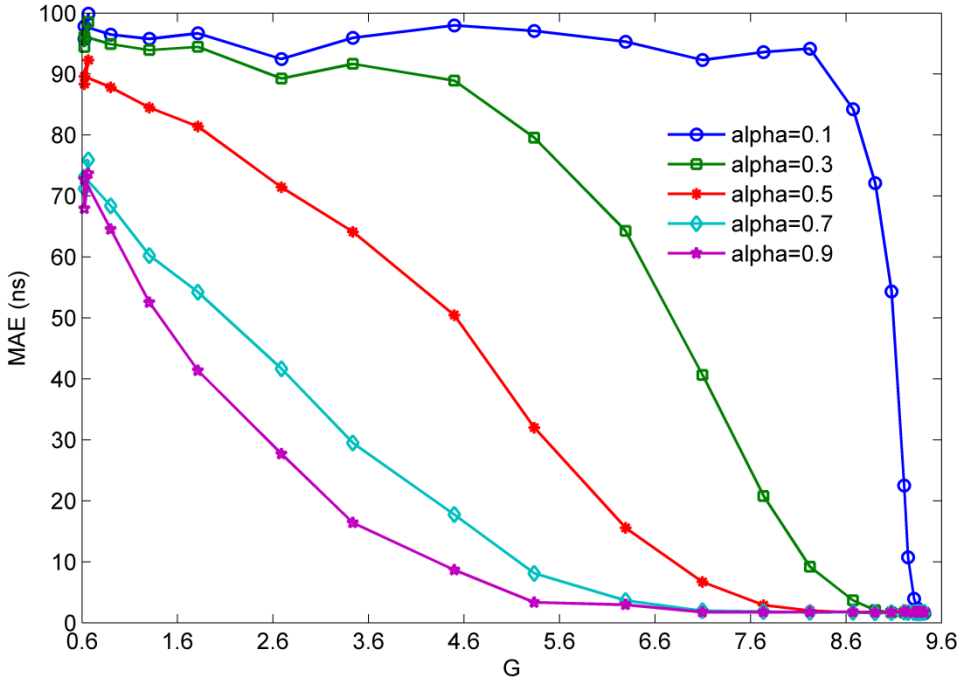

Figure 16. MAE with Respect to G(CM1.1 and Tb=3ns)

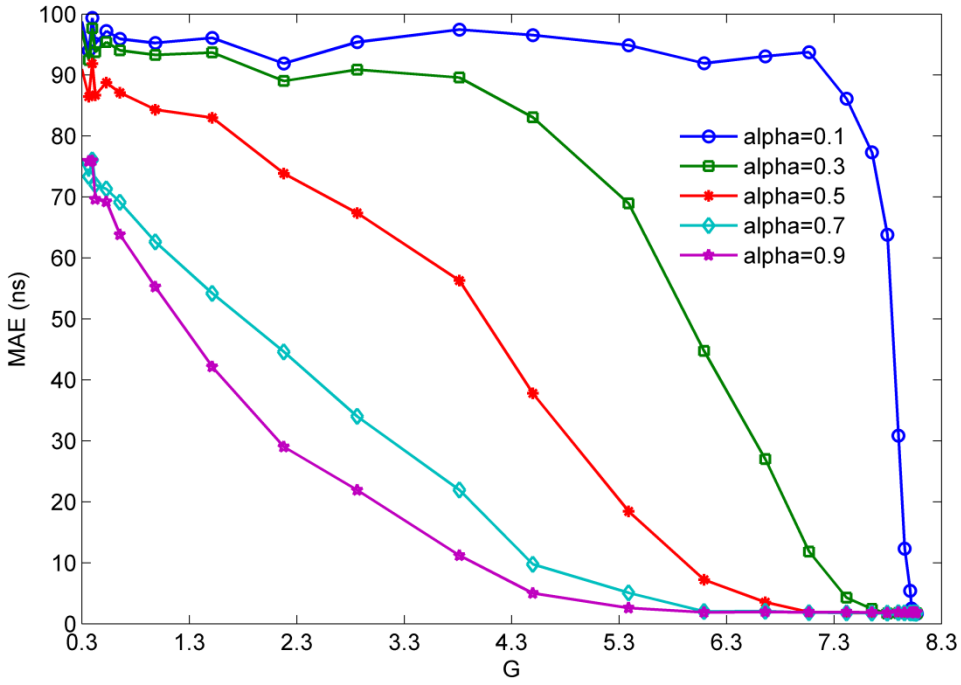

Figure 17. MAE with Respect to G(CM1.1 and Tb=4ns)

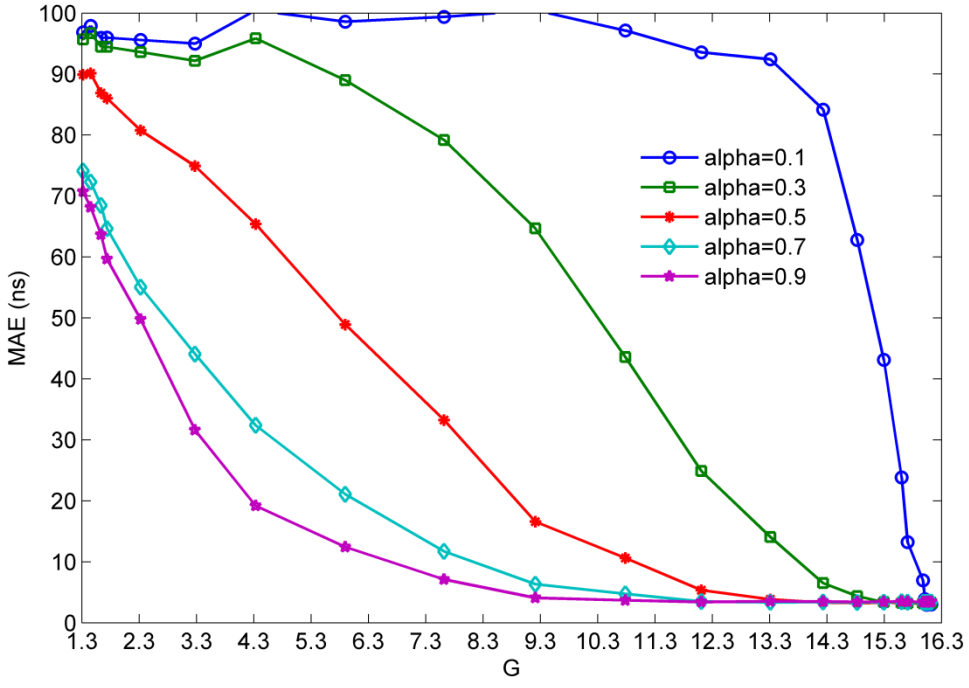

Figure 18. MAE with Respect to G(CM2.1 and Tb=1ns)

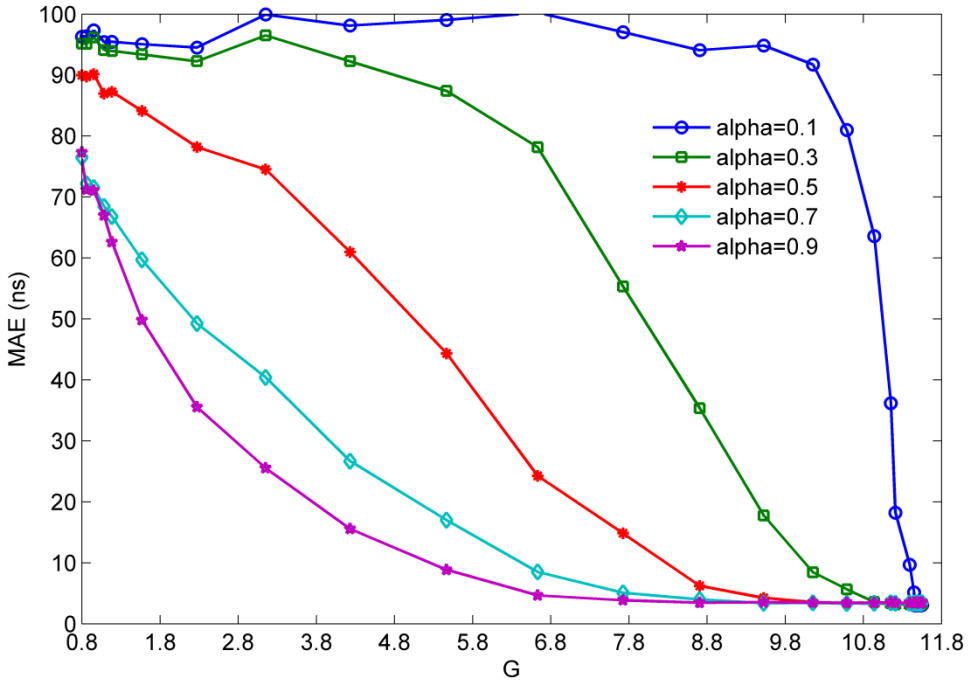

Figure 19. MAE with Respect to G (CM2.1 and Tb=2ns)

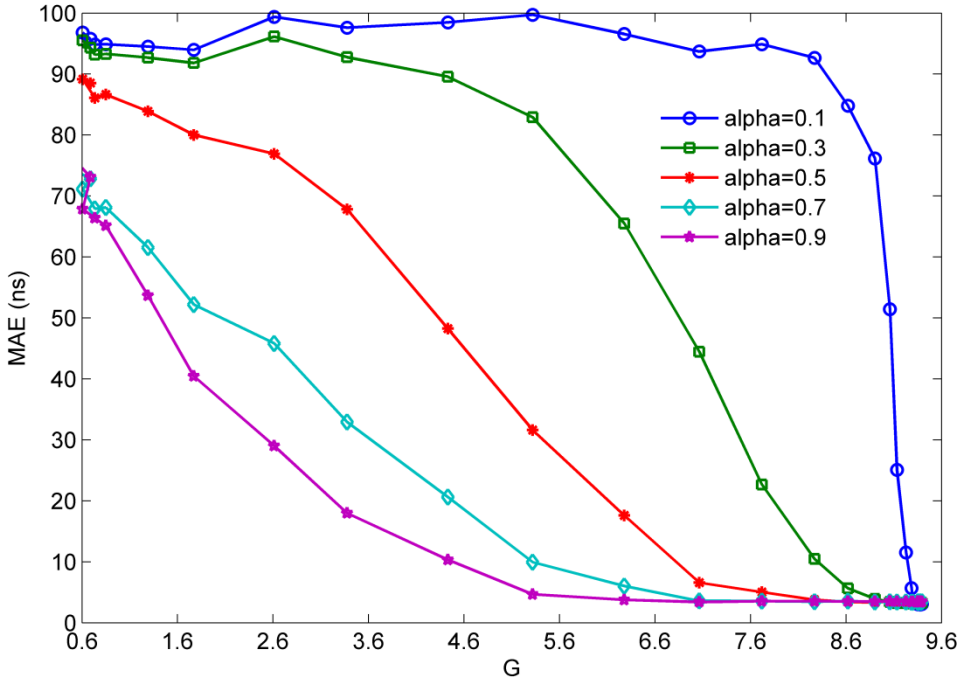

Figure 20. MAE with Respect to G(CM2.1 and Tb=3ns)

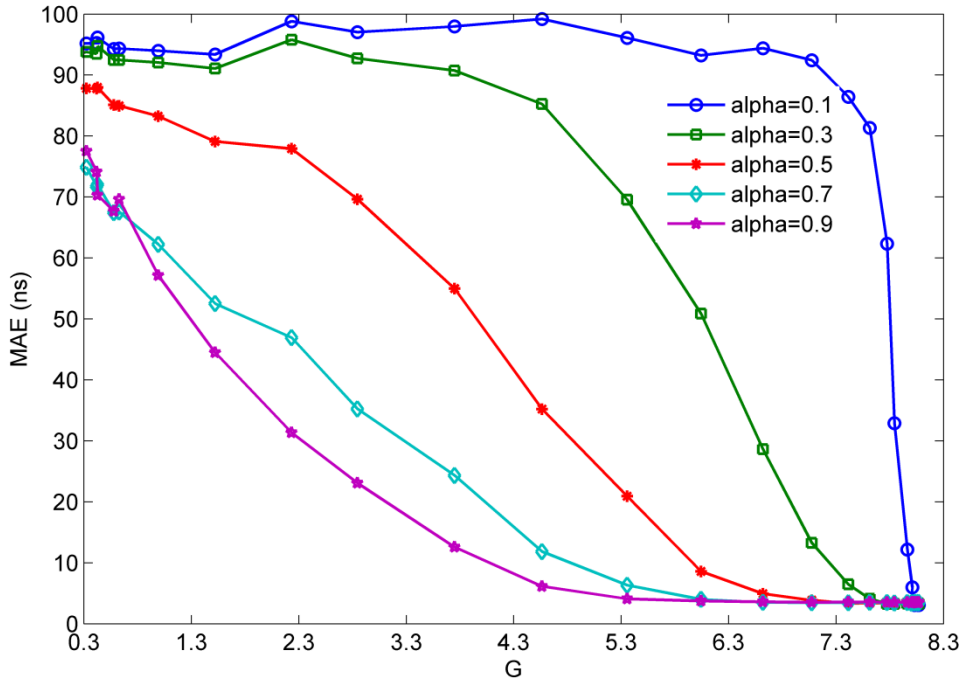

Figure 21. MAE with Respect to G(CM2.1 and Tb=4ns)

5.3. Optimal Thresholds

The normalized threshold α_{norm} with respect to the minimum MAE is called the best threshold α_{best} for a given G. Therefore, the lowest points of the curves in Figures 14-21for each G are selected as the α_{best} .

These results show that the relationship between the two parameters is not affected significantly by the channel model, but is more dependent on the integration period, so the values for channels CM1.1 and CM2.1 can be combined. Therefore, the average of the two values is used as the optimal normalized threshold

$$\alpha_{opt}^{(Tb=1ns)}(G) = \frac{\alpha_{best}^{(CM\,1.1,\,Tb=1ns)}(G) + \alpha_{best}^{(CM\,2.1,\,Tb=1ns)}(G)}{2} \quad (21)$$

$$\alpha_{opt}^{(Tb=2ns)}(G) = \frac{\alpha_{best}^{(CM\,1.1,\,Tb=2ns)}(G) + \alpha_{best}^{(CM\,2.1,\,Tb=2ns)}(G)}{2} \quad (22)$$

$$\alpha_{opt}^{(Tb=3ns)}(G) = \frac{\alpha_{best}^{(CM\,1.1,\,Tb=3ns)}(G) + \alpha_{best}^{(CM\,2.1,\,Tb=3ns)}(G)}{2} \quad (23)$$

$$\alpha_{opt}^{(Tb=4ns)}(G) = \frac{\alpha_{best}^{(CM\,1.1,\,Tb=4ns)}(G) + \alpha_{best}^{(CM\,2.1,\,Tb=4ns)}(G)}{2} \quad (24)$$

5.4. Normalized Threshold with G

From the results in the previous section, the relationship between α_{best} and G shows in Figure 22 (1ns), Figure 23 (2ns), Figure 24 (3ns) and Figure 25 (4ns) for each value of G. This shows that the relationship between the two parameters is not affected significantly by the CM, but is more dependent on the integration period. Therefore, four piecewise functions were fitted to these results aiming at $Tb = (1ns, 2ns, 3ns, 4ns)$. The relationship can be described as expression (25), expression (26), expression (27) and expression (28).

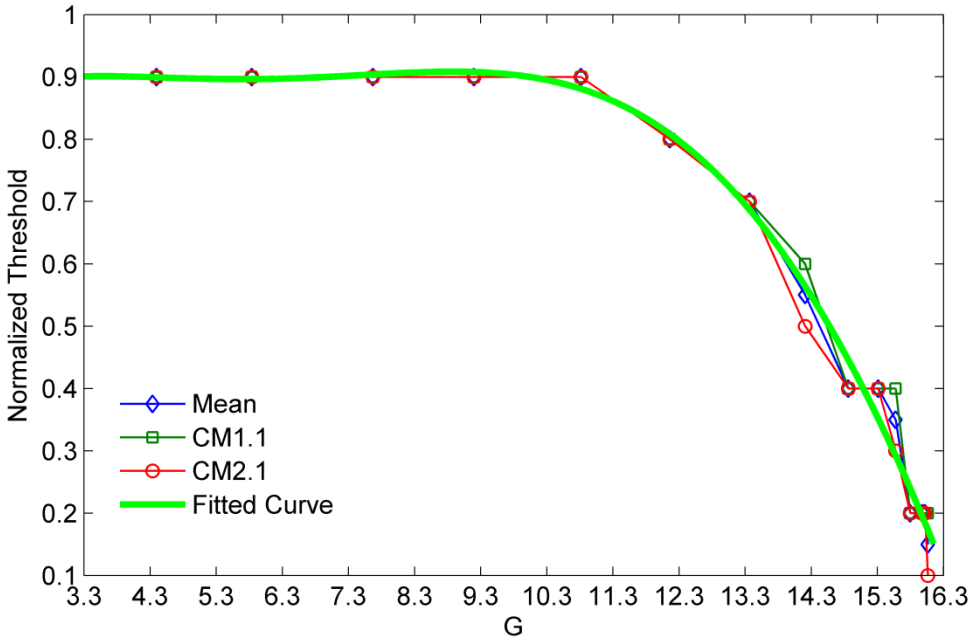

Figure 22. Normalized Threshold with Respect to GTb=1ns

$$\alpha_{best} = \begin{cases} 0.8 & x < 3.3 \\ 7.49e^{-6}x^5 - 3.887e^{-4}x^4 + 6.575e^{-3}x^3 - 0.0483x^2 + \\ 0.1582x + 0.7116 & 3.3 \le x < 16.3 \\ 0.1 & 16.3 \le x \end{cases} \quad (25)$$

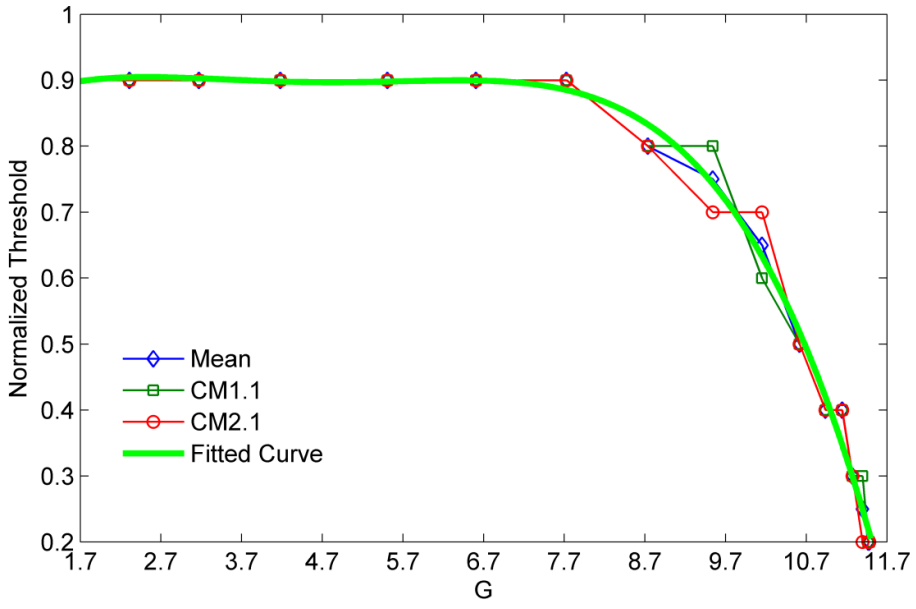

Figure23. Normalized Threshold with Respect to GTb=2ns

$$\alpha_{best} = \begin{cases} 0.8 & x < 1.7 \\ -3.559e^{-4}x^4 + 6.532e^{-3}x^3 - 4.226e^{-2}x^2 + \\ 0.1115x + 0.802 & 1.7 \le x < 11.2 \\ 0.1 & 11.2 \le x \end{cases} \quad (26)$$

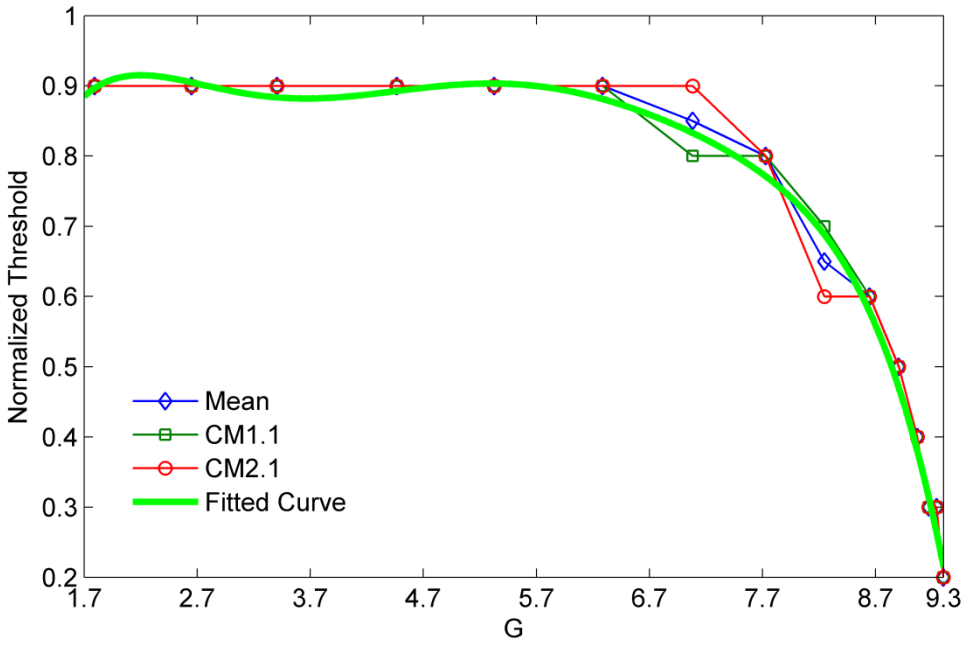

Figure24. Normalized Threshold with Respect to GTb=3ns

$$\xi_{best} = \begin{cases} 0.8 & x < 1.7 \\ -1.803e^{-4}x^6 + 5.729e^{-3}x^5 - 7.324e^{-2}x^4 + 0.4759x^3 - \\ 1.639x^2 + 2.806x - 0.9518 & 1.7 \le x < 9.3 \\ 0.1 & 9.3 \le x \end{cases} \quad (27)$$

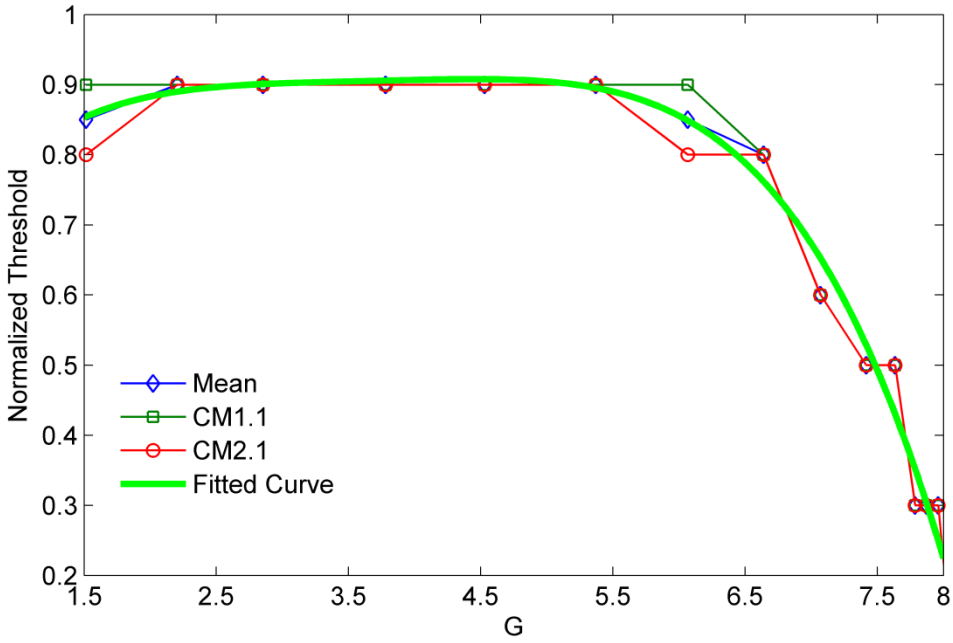

Figure25. Normalized Threshold with Respect to GTb=4ns

$$\xi_{best} = \begin{cases} 0.8 & x < 1.5 \\ -1.952e^{-3}x^4 + 0.02852x^3 - 0.1564x^2 + \\ 0.3859x + 0.54 & 1.5 \le x < 8 \\ 0.1 & 8 \le x \end{cases} \quad (28)$$

6. Results and Discussion

In this section, the MAE is examined for different TOA estimation algorithms which based on Energy Detecting in the IEEE 802.15.3cCM1.1 and CM2.1 channels. As before, 1000 channel realizations are generated for each case. A 2PPM-TH-60GHz signal is employed, and the received signal is sampled at $f_c = 1 \cdot e^{10}$ Hz. The other system parameters are $T_f = 200ns$, $T_c = 1ns$ the value of Tb is from 1ns to 4nsand N = 1. Each realization has a TOA uniformly distributed within (0- T_f).

The MAE for SNR values from 4dB to 34dB in LOS (CM1.1) is presented in the Figure26 ($Tb = 1ns\ and\ 4ns$) and Figure 28 ($Tb = 2ns\ and\ 3ns$). At the same time, The MAE for SNR values from 4dB to 34dB in NLOS(CM2.1) is presented in the Figure 27($Tb = 1ns\ and\ 4ns$)and Figure29($Tb = 2ns\ and\ 3ns$). This shows that the proposed algorithm performs even much better than other algorithm such as MES and Fixed Threshold. The performance in CM1.1 is better than in CM2.1 aiming at the same Tb . In most cases, the performance with $Tb = 1ns$ is better than that with $Tb = [2ns, 3ns\ and\ 4ns]$ regardless of the channel. The MAE performance with three TOA algorithms in channels CM1.1 and CM2.1 are shown in Figures 26-29respectively.

Here “MES” is the Maximum Energy Selection algorithm, and the normalized threshold for the Fixed Threshold algorithm is set to 0.4 and 0.6. The MAE with the proposed algorithm is lower than other algorithms, particularly at low to moderate SNR values. The proposed algorithm is better except when the SNR is greater than 19dB. The performance of the proposed algorithm is more robust than the other algorithms, as the performance difference is very small compared to the difference with other algorithms. For almost all SNR values the proposed algorithm is even much better. Conversely, the

performance of other algorithms varies greatly and is very bad for low to moderate SNR values.

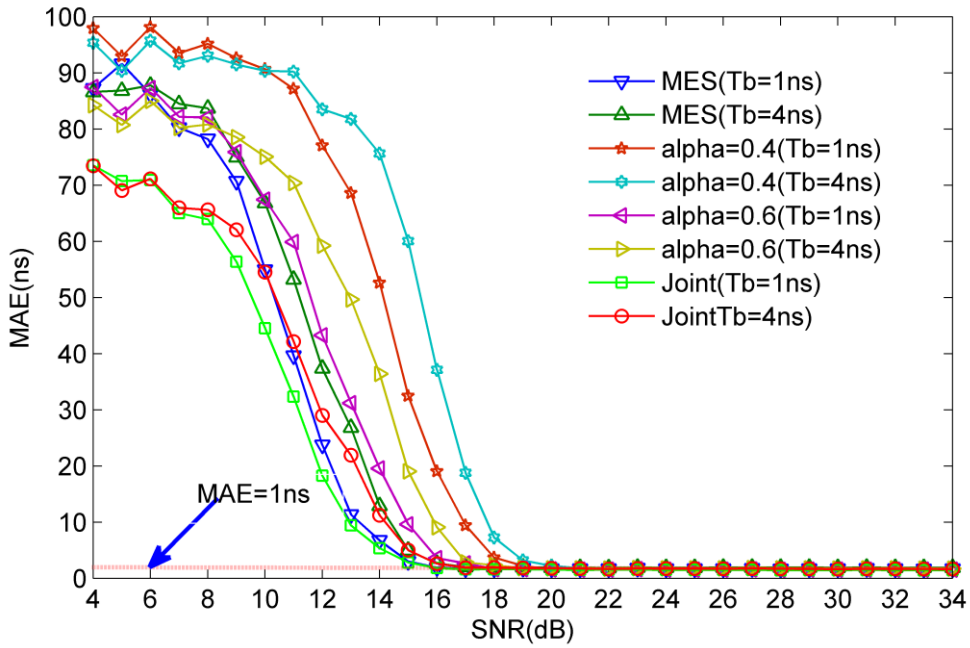

Figure26. MAE for Different Algorithms with CM1.1 (Tb=1ns and 4ns)

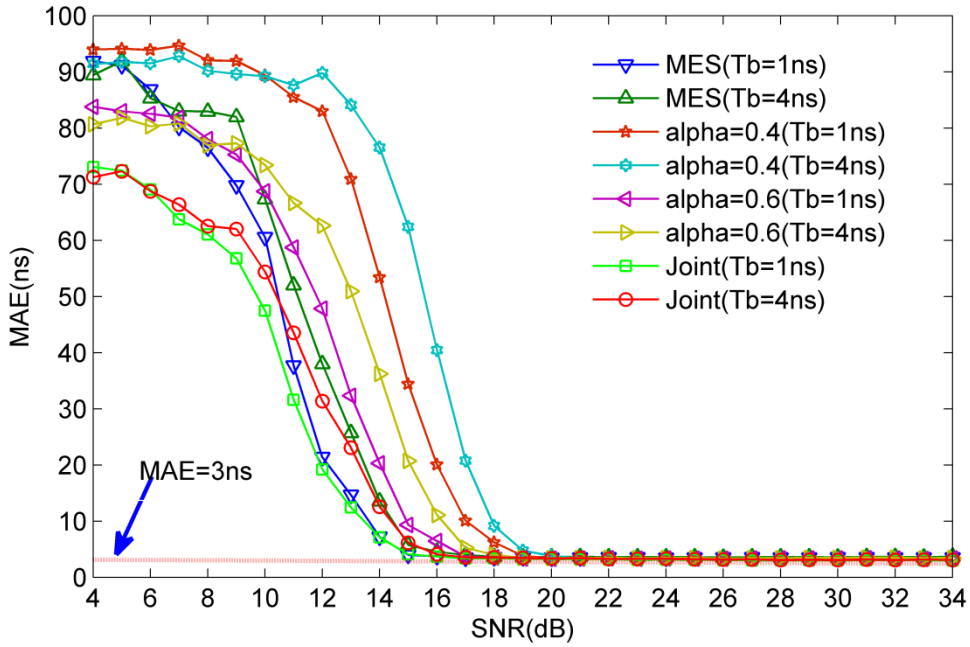

Figure27. MAE for Different Algorithms with CM1.1 (Tb=2ns and 3ns)

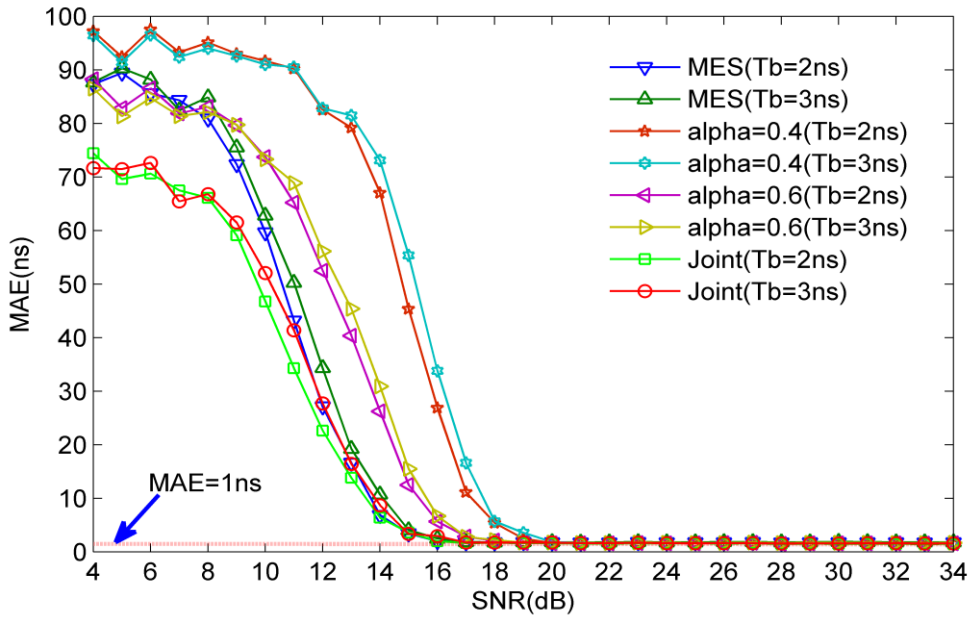

Figure 28. MAE for Different Algorithms with CM2.1 (Tb=1ns and 4ns)

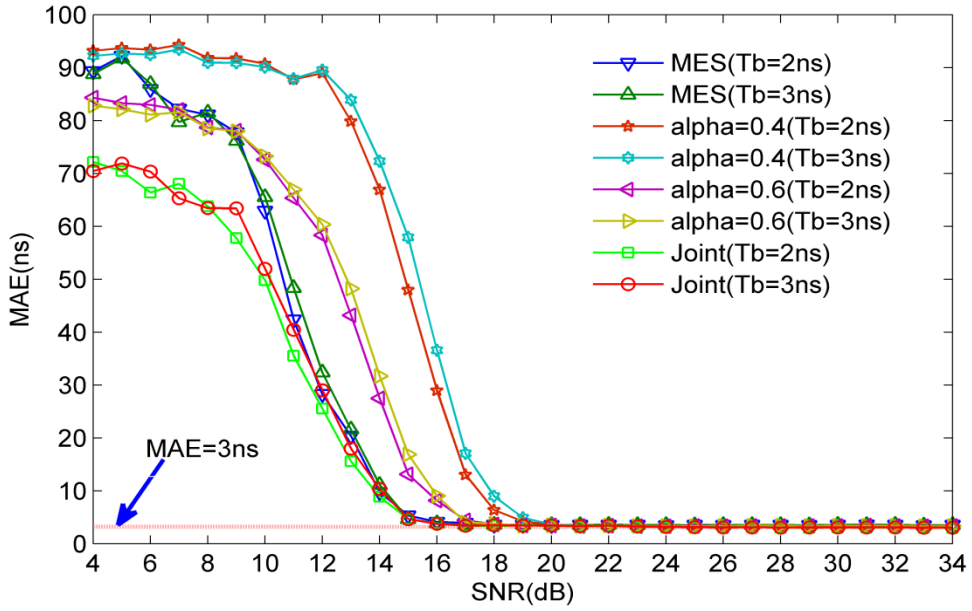

Figure 29. MAE for Different Algorithms with CM2.1 (Tb=2ns and 3ns)

7. Conclusion

Low complex TOA estimation algorithms that based on Energy Detector have been examined for IR-60GHz ranging, positioning, and tracking applications. Statistical parameters were investigated and a joint metric based on Skewness, Kurtosis, Maximum Slope and Standard Deviation was developed for Threshold Crossing TOA estimation according to the results obtained. The best normalized threshold was determined using simulation with the CM1.1 and CM2.1 channels. The effects of the integration period and channel model were investigated. It was determined that the proposed threshold selection

technique is largely independent of the channel model. The performance of the proposed algorithm was shown to be better than several known algorithms. In addition, the proposed algorithm is more robust to changes in the SNR and integration period.

Acknowledgments

The authors would like to thank colleagues from the UWB Laboratory in the College of Information Science and Engineering, Ocean University of China, for help with obtaining the measurement data. This work was supported by the Nature Science Foundation of China under Grant No. 60902005, the Qingdao International Science and Technology Cooperation Projects of Qingdao under Grant No. 12-1-4-137-hz, and the Qingdao Transformation of Scientific and Technological Achievements Guiding Plan (youth special program) under Grant No. 14-2-4-37-jch.

References

[1] L. Zhang, "A fully integrated 60GHz five channel CMOS receiver with 7GHz ultra-wide band width for IEEE 802.11ad standard", Communication, China, vol. 11, no. 6, **(2014)**, pp. 42-50.
[2] S. K. Yong and C. C. Chong, "An overview of multigigabit wireless through millimeter Wave Strategy: Potentials and Technical Challenges", EURASIP J. Wireless Communications and Networking, vol. 2007, no. 1, **(2007)**, pp. 1-10.
[3] R. C. Daniels and R. W. Heath, "60 GHz wireless communications: emerging requirements and design recommendations", IEEE Vehicular Strategy Society, vol. 2, **(2007)**, pp. 41-50.
[4] C. C. Chong, F. M. Peter, Smulders, et al, "60GHz-Millimeter-Wave Radio Principle, Strategy, and News Results", EURASIP Journal on Wireless Communications and Networking, vol. 2007, no. 1, **(2007)**, pp. 1-8.
[5] S. K. Yong, P. F. Xia P F and Alberto V G, "60-GHz Strategy for Gbps WLAN and WPAN: From Theory to Practice", Beijing: Press of China Machine, **(2013)**.
[6] R. C. Daniels and R. W. Health, "60 GHz wireless communications: emerging requirements and design recommendations", IEEE Vehicular Strategy Magazine, vol. 2, no. 3, **(2007)**, pp. 41-50.
[7] D. Jie, X. Cui, H. Zhang, and G. Wang, "An ultra-wideband location algorithm based on neural network". International Conference on Wireless Communications Networking and Mobile Computing (WiCOM), vol. 11, no. 6, (**2010)**, pp. 56-64.
[8] X. Tu, H. Zhang, X. Cui and T. A. Gulliver, "3D TDOA/AOA location based on extended Kalman filter", International Symposium on Antennas, Propagation and EM Theory (ISAPE), vol. 11, no. 6, (**2010)**, pp. 56-64.
[9] Z. Sahinoglu and S. Gezici, "Ranging in the IEEE 802.15.4a standard", in IEEE Wireless and Microwave Strategy Conference (WAMICON), **(2006)**.
[10] D. Dardari, A. Conti, U. Ferner, A. Giorgetti, and M. Z. Win, "Ranging with ultra-wide bandwidth signals in multipath environments", Proceedings of the IEEE, vol. 97, no. 2, (**2009)**, pp. 404-426.
[11] Y. Zhang, A. K. Brown, W. Q. Malik, and D. J. Edwards, "High resolution 3D angle of arrival determination for indoor UWB multipath propagation", IEEE Transactions on Wireless Communications, vol. 7, no. 8, **(2010)**, pp. 3047-3055.
[12] D. Dardari, A. Giorgetti, and M.Z. Win. "Time of arrival estimation of UWB signals in the presence of narrowband and wideband interference", IEEE International Conference on Ultra-Wideband (ICUWB), **(2007)**.
[13] M. Bocquet, C. Loyez, and A. BenlarbiDelai, "Using enhanced TDOA measurement for indoor localization", IEEE Microwave and Wirele SG Components Letters, vol. 15, no.10, **(2005)**, pp. 612-614.
[14] A. Abbasi and M.H. Kahaei, "Improving source localization in LOS and NLOS multipath environments for UWB signals". International CSI Computer Conference (CSICC), **(2009)**.
[15] I. Guvenc and Z. Sahinoglu, "Multi-scale energy products for TOA estimation in IRUWB systems", IEEE Global Telecommunications Conference, (GLOBECOM), **(2005)**.
[16] A. Y.Z. Xu, E. K. S. Au, A. K.S. Wong, and Q. Wang, "A novel threshold based coherent TOA estimation for IR-UWB systems", IEEE Transactions on Vehicular Strategy, vol. 58, no. 8, **(2009)**, pp. 4675-4681.
[17] I. Guvenc and Z. Sahinoglu, "Threshold selection for UWB TOA estimation based on kurtosis analysis", IEEE Communications Letters, vol. 9, no. 12, **(2005)**, pp. 1025-1027.
[18] I. Guvenc and Z. Sahinoglu. "Threshold based TOA estimation for impulse radio UWB systems", IEEE International Conference on Ultra-Wideband,**(2005)**.
[19] "IEEE Standard for Information strategy--Local and metropolitan area networks--Specific requirements--Part 15.3: Wireless Medium Access Control (MAC) and Physical Layer (PHY) Specifications for High Rate Wireless Personal Area Networks (WPAN) amendment

2:millimeter-wave-based alternative physical layer extension". IEEE Computer Society, IEEE 802.15.06-0474-00-003c, **(2009)**.
[20] "802.11n-2009-IEEE Standard for Information strategy-- Local and metropolitan area networks--Specific requirements--Part 11: Wireless LAN Medium Access Control (MAC) and Physical Layer (PHY) Specifications Amendment 5: Enhancements for Higher Throughput", IEEE Computer Society, IEEE 978-0-7381-6731-2, **(2009)**.
[21] C. R. Andersonn and T. S. Rappaport, "In-building wideband partition loss measurements at 2.5 and 60GHz", IEEE Transactions on Wireless Communications, vol. 3, no. 3, **(2004)**, pp. 922-928.
[22] S. Collong, G. Zaharia and G. E. Zein, "Influence of the human activity on wide-band characteristics of the 60GHz indoor radio channel", IEEE Transactions on Wireless Communications, vol. 3, no. 6, **(2005)**, pp. 2396-2406
[23] A. Maltsev, R. Maslennikov and A. Sevastyanov, "Experimental investigations of 60GHz WLAN systems in office environment", IEEE Journal on Selected Areas in Communications, vol. 27, no. 8, **(2009)**, pp. 1488-1499.
[24] M. G. Sanchez, A. V. Alejos and I. Cuinas, "Comparision of space diversity performance in indoor radio channels at 40GHz and 60GHz", Proc. of European Conference on Wireless Strategy, Amsterdam, **(2008).**
[25] H. B. Yang, "Channel characteristics and transmission performance for various channel configurations at 60GHz", EURASIP Journal on Wireless Communications and Networking, vol. 2007, no. 1, **(2007)**, pp. 43-43.
[26] N. Li, "Study on the properties of 60 GHz impulse radio communication system". Qingdao: Ocean University of China, **(2012)**.
[27] X. Cui, C. Wu and J. Li, "UWB simulation of energy detection algorithm based on the Internet of things", Application of micro-computer, vol. 27, no. 9, **(2011)**, pp. 20-26.

Authors

Xiao-Lin Liang now studies in College of Information Science and Engineering and is a Ph. D. candidate in Ocean University of China. His research interests include ultra-wideband radio systems, 60GHz wireless communication system.

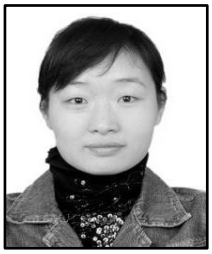

Ting-Ting Lu, She received the Ph. D. degree in College of Information Science and Engineering from Ocean University of China in 2013. She is now a lecture in College of Information Science and Engineering. Her research interests include ultra-wideband radio systems, 60GHz wireless communication system.

Hao Zhang, He received the MBA degree in New York Institute of Technology, American in 2001 and the Ph. D. degree in Electrical and Computer Engineering from the University of Victoria, Canada in 2004. He was a Project Manager for Microsoft Inc. in United States during January 2000-May 2000. During 2004-2008, he was the Vice President for the United States Gamma Capital Inc. He is now an Adjunct Assistant Professorin the Department of Electrical and Computer Engineering. Also he becomes a professor and the Ph. D. supervisor in College of Information Science and Engineering from Ocean University of China in 2006. His research concerns ultra-wideband radio systems, 60GHz wireless communication system and MIMO wireless communication.

Luji Cui, He now studies in College of Information Science and Engineering and is a master candidate in Ocean University of China. His research interests include ultra-wideband radio systems, 60GHz wireless communication system.

T. Aaron. Gulliver, He received the Ph. D. degree in Electrical and Computer Engineering from the University of Victoria, Canada in 1989. He is now a professor and the Ph. D. supervisor in the Department of Electrical and Computer Engineering. In 2002, he becomes a Fellow of the Engineering Institute of Canada, and in 2012 a Fellow of the Canadian Academy of Engineering. He is also a senior member of IEEE. His research concerns information theory and communication theory, algebraic coding theory and smart grid and ultra wideband communication.